CHAPTER I
Context of the research

CHAPTER I
CONTEXT OF THE RESEARCH

This chapter begins by setting the context of the research with the problematic of the greenhouse gas emissions linked to the global warming. Hydrogen is then proposed as an alternative to the use of fossil fuels and the photoelectrolysis of water is envisaged as a green way to produce it. This is followed by the presentation of hematite as a promising material for the photoanode in water splitting. Finally, the objectives and the content of the different chapters are described.

I.1 Problematic [1,2]

Since the preindustrial period, the temperature on Earth has been growing up more importantly. The global warming has many negative impacts (Figure I-1) both on natural and human systems (on all the continents and in the oceans).

It generates extreme climatic phenomena such as heavy precipitations, droughts and storms.

The ecosystem does not have the natural ability to change its geographical extension following the fast pace of these changes. Some plant and animal species are then threatened.

Moreover, some human populations could have to move in order to escape different issues caused by the climatic changes. The global warming generates the melting of polar ice caps and increases the sea level. This can induce the migration of the population currently living near the coast.

The global warming can also have a real impact on the food safety. Actually, marine biodiversity is sensitive to the ocean pH which is decreasing because of the CO_2 concentration increase and some aquatic species are threatened. This can affect the fishing yield. The cultivation of wheat, rice or corn can also be affected in the tropical region.

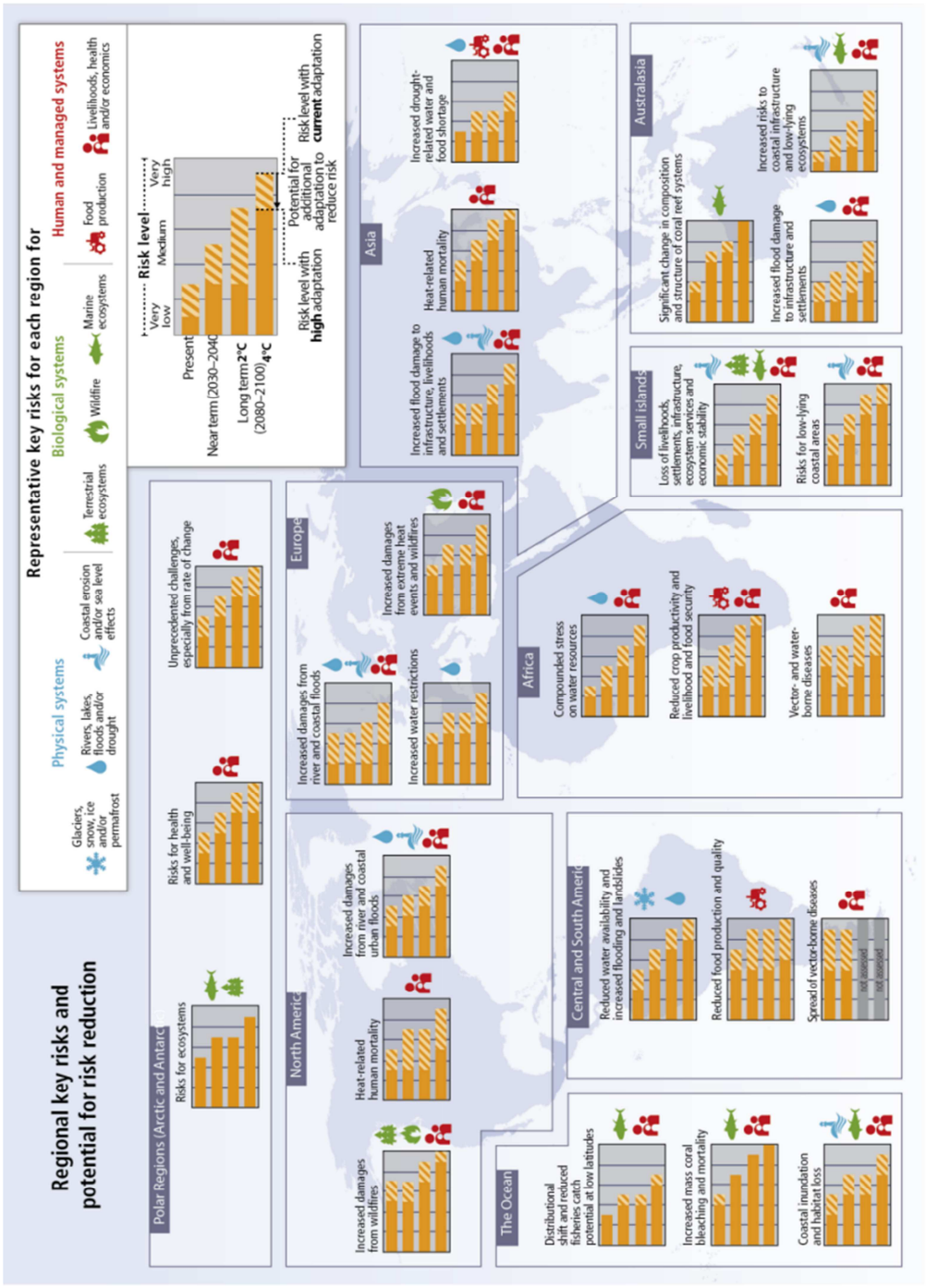

Figure I-1: Diagram showing regional key risks and their level in the present and the future as a function of the limitation of the global warming to 2°C or 4°C since the preindustrial period[1].

The global warming is due to higher greenhouse gas (GHG) emissions such as CO_2, CH_4, SO_2 and N_2O since the preindustrial period (1750). The GHG emissions rise mainly comes from human activities and is not only due to the industries development and the use of fossil fuels but is also linked to land use, lifestyle, energy consumption, etc. Between 1750 and 2011, CO_2 emissions have been estimated to 2040 ± 310 Gt of which half for the last 40 years. About 40% are still present in the atmosphere and about 30% have been absorbed by the oceans causing an acidification of the water[1]. The remaining part has been stored in plants and in the soil.

To limit the negative impacts of the global warming, a coordinated global scale action is necessary to limit greenhouse gas emissions everywhere on Earth because these gases accumulate over time and mix worldwide. The most optimistic perspective for 2100 is to limit the global mean temperature change since 1870 at 2°C (2°C scenario). Until now, the mean temperature change is about 0.6°C. Among the GHG emissions, the anthropogenic CO_2 emissions must be reduced.

Figure I-2 shows different scenarios (ellipses) depending on the CO_2 emissions. The light blue, dark blue and yellow involves a decrease of the GHG emissions which implies long-term and sustainable development rather than short term strategies.

In order to reach the 2°C scenario, efforts are needed in different sectors such as power generation, industry and transport. These efforts should limit the risks from climate change.

Concerning the power sector, different technologies can be used to limit the CO_2 emissions. The nuclear power is one of them but the safety must be improved and new process in the radioactive waste treatment must be found.

The natural gas-fired power and the coal-fired power are also considered in some countries but they have to be coupled to carbon capture and storage (CCS) systems. The process preferentially used depends on the resources of the countries.

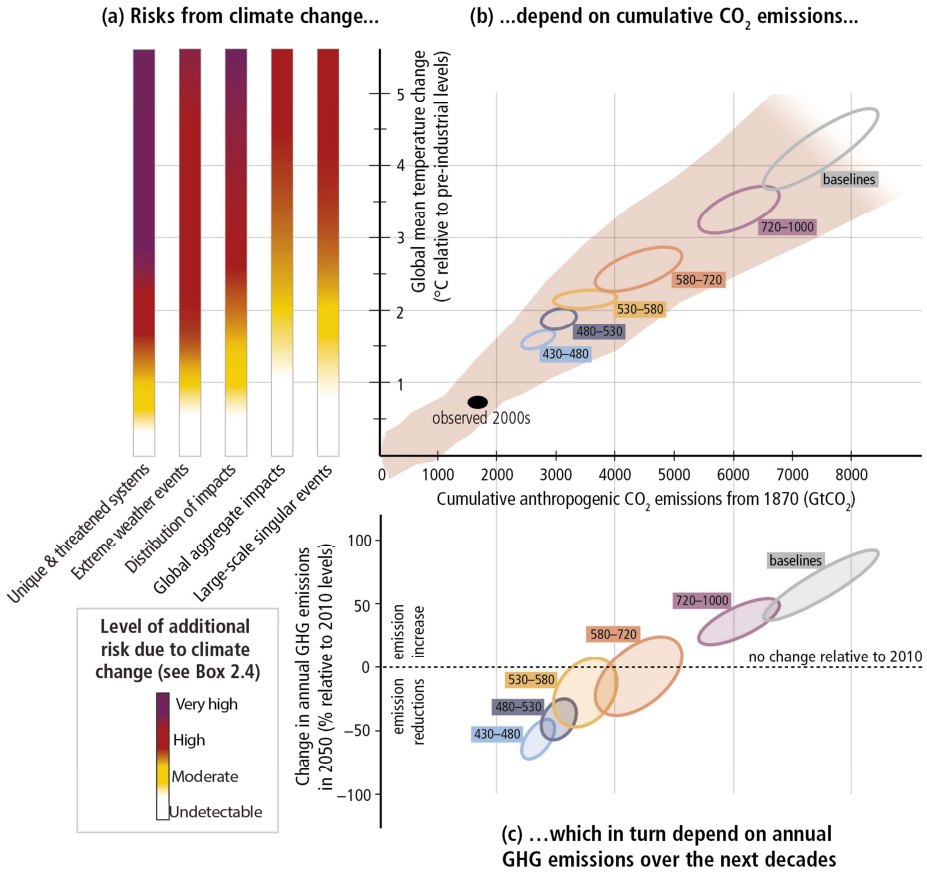

Figure I-2: Estimation of the level of risks linked to the global warming as a function of the evolution of the GHG emissions. Ellipses represent different scenarios[1].

Another power generation technology developed is the renewable energies which must be further improved to be competitive in terms of cost and yield compared to existing power sources. An issue with this type of power generation is their daily and seasons efficiency fluctuations. This justifies the development of energy storage technologies and smart grids that must be associated to this type of power generation.

In industries, the energy demand is huge. Hence, they try to reduce the energy demand with, for example, co-generation system and they look for alternatives to their fuel consumption as for example the use of biofuel instead of fossil fuel.

The transport accounted for 28% of overall energy consumption and led to emissions of 8.7Gt CO_2 in 2012[3]. Passenger transport accounts for nearly 60% of total transport demand and the aviation represent only 18% of the passenger transport[3]. In the nearer term, we have to choose more efficient transport modes (buses…) and to reduce our trips by encouraging, for example, the homeworking and the video conferences[2]. In a longer term perspective, alternatives to the fossil fuel use must be found for this field.

Electric vehicles are already present in the market. These vehicles are interesting for short trips because of the battery capacity. Indeed, the vehicle is stopped during the charge of the battery and this can be an issue for longer trips.

Another alternative to fossil fuels is biofuels. However, if the demand in biofuels is growing up, the use of plants as fuel will be in competition with the food production.

To avoid this issue with biofuels, another fuel is considered: hydrogen. It can be burned directly or it can be combined with a fuel cell to be converted into electricity. Vehicles using this last technology are called Fuel Cell Electric Vehicles (FCEVs). The price of the two first FCEVs commercially available (Huyndai ix35 and Toyota Mirai) is around 60000-70000 euros in Europe. This price depends on the cost of the fuel cell and the storage system for hydrogen. Improvement in the development of each element composing FCEVs must be done to reduce the global price[2].

Nevertheless, in order to make these alternatives competitive compared to fossil fuels and encourage the deployment of new technologies; governments need to introduce new policies as for example carbon pricing. Moreover, campaigns and educational programs must be developed to increase the awareness-raising of the population. Finally, a mass production would considerably reduce the price of FCEVs.

I.2 Hydrogen [2]

If generated from a low-carbon footprint technology, hydrogen is a fuel that can reduce air pollution and GHG emissions compared to fossil fuels. It is a flexible energy carrier that can be transformed in power or heat without GHG emissions since the only reaction product is water. We can use, for example, a fuel cell to generate electricity from hydrogen and oxygen. It can also be a link between energy supply and demand (Figure I-3) particularly in off-grid regions.

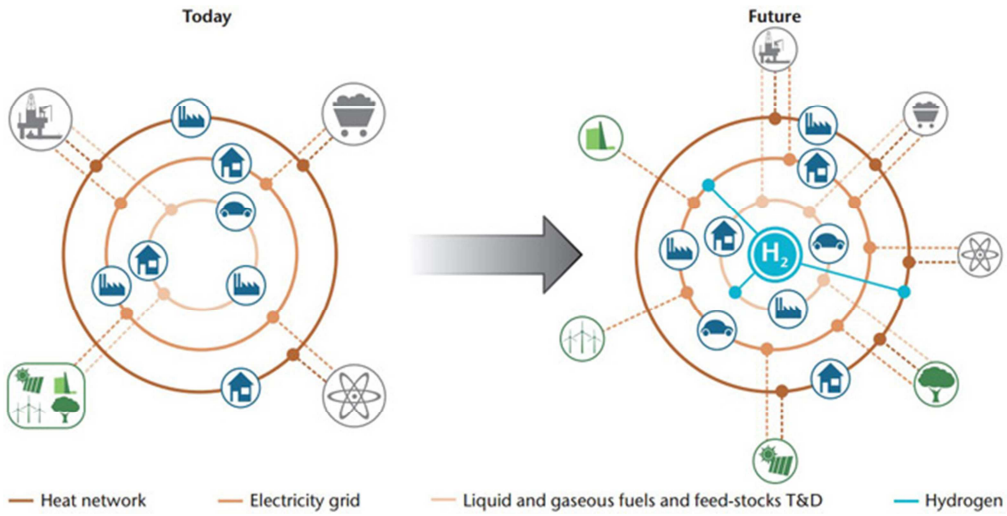

Figure I-3: Energy system today and the possibility in the future[2].

Hydrogen makes possible the storage of energy produced by renewable source such as photovoltaic panels and wind turbines. These energy sources vary irregularly over the day, the seasons and the place on Earth. Therefore, it is important to find storage system to associate with them. Batteries can be used but for stationary applications only. The advantage of hydrogen is its ability to be transported to another place where there is a demand in energy. For example, hydrogen is particularly suitable in the transport field for FCEVs.

I.2.1 An application of hydrogen: FCEVs

FCEVs are vehicles using hydrogen stored on board in a pressurized tank and a fuel cell to convert hydrogen into electricity. But they are also hybrid vehicles because they need a battery to retrieve the braking energy which will be used to reduce the peak of demand from the fuel cell during the acceleration.

In 2014, 192 FCEVs (passengers' cars and buses) were already running in Europe in several demonstration projects[1]. The ix35 Fuel Cell[4] (Figure I-4) is the first mass production model of Huyndai with two 700bar hydrogen tank. This car has a power of 136hp (≈100kW) and an operating range of 594km per charge. This means that the consumption in fuel of this car is 3.6L of H_2/100km. This example shows that the technology is available.

Some improvements must be done particularly in the field of fuel cells and H_2 tanks to reduce the cost of this type of vehicles[5]. A higher demand on the market could also reduce the cost. However, in order to increase the demand, hydrogen refueling stations must be developed. In 2015, 82 hydrogen refueling stations were operated in Europe, 63 in North America, one in South America, and 38 in Asia as showed on the map (Figure I-5) (results given by "H2stations.org").

Actually, the production and the distribution of hydrogen have to be taken into account in the development of FCEVs.

[1] A timeline of all hydrogen vehicles worldwide is available on "H2mobility.org".

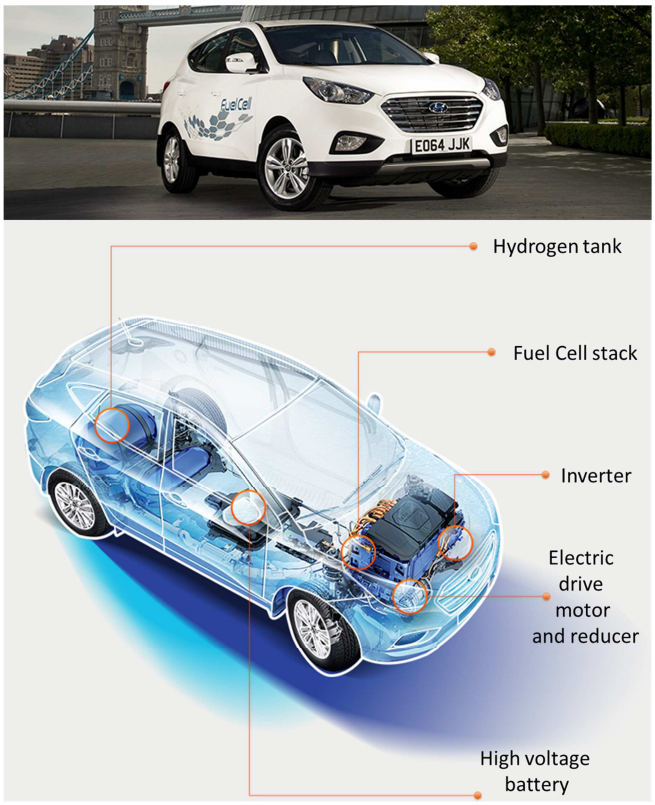

Figure I-4: (Up) A photography of the ix35 Fuel Cell (the first mass production model of Huyndai) and (Down) the key parts of the motion technology[4].

Figure I-5: Hydrogen refueling stations worldwide. Statistics and maps were provided by Ludwig-Bölkow-Systemtechnik©.

I.2.2 Distribution of hydrogen

Two alternatives exist for the distribution of hydrogen: the production of hydrogen at the refueling station or in a central production plant. But for this last option, hydrogen must be transported up to the refueling station. The centralized production of hydrogen offers economies of scale but the transport increases the costs. Two different transports exist: trucks (for gaseous or liquid hydrogen) or pipelines. The choice of the means of transport depends on the location of the refueling station compared to the centralized hydrogen production and the hydrogen demand in the area of the refueling station must also be taken into account. For example, the daily refueling capacity of a station in a small city will be lower than in a big city.

I.2.3 Production of hydrogen

Different technologies of hydrogen production exist. To date, hydrogen is not used as an energy carrier but rather as feedstock to produce new molecules in the chemical industries[6] (NH_3 or CH_3OH for example) or in refining industries.

Currently, the steam gas reforming method from natural gas or methane is the most used production method followed by coal gasification[7]. The problem with these processes is their carbon footprint due to the fuels used for the heating and the CO_2 released during the process[8]. This is contradictory with the use of hydrogen as fuel to reduce the GHG emissions. This explains that new technologies are developed to produce hydrogen. The splitting of water into hydrogen and oxygen by electrolysis is one of the alternatives to the steam gas reforming.

Electric power is necessary to achieve the electrolysis of water. The electric power can be provided by different sources. To reduce CO_2 emissions, the renewable sources are favored. As mentioned before, renewable energy sources vary irregularly over the day, the seasons and the place on earth. Therefore, the production of energy does not match directly the demand. Therefore, storage systems must be developed. One approach consists to store energy from renewable sources in hydrogen bonds by using an electrolyser.

Electrolysers are composed of stacks comprising up to 100 cells and, therefore, are very flexible systems that can be adapted for a lot of different applications. Alkaline and Proton Exchange Membrane (AEM and PEM) electrolysers are already commercialized but some new electrolysers are in development as for example Solid Oxide Electrolyser Cell (SOEC) to reduce the cost and improve the efficiency[9]. Figure I-6 shows the principle of these different electrolysis cells.

In order to reduce the demand in electric power for splitting water into oxygen and hydrogen, an alternative is the photoelectrolysis of water.

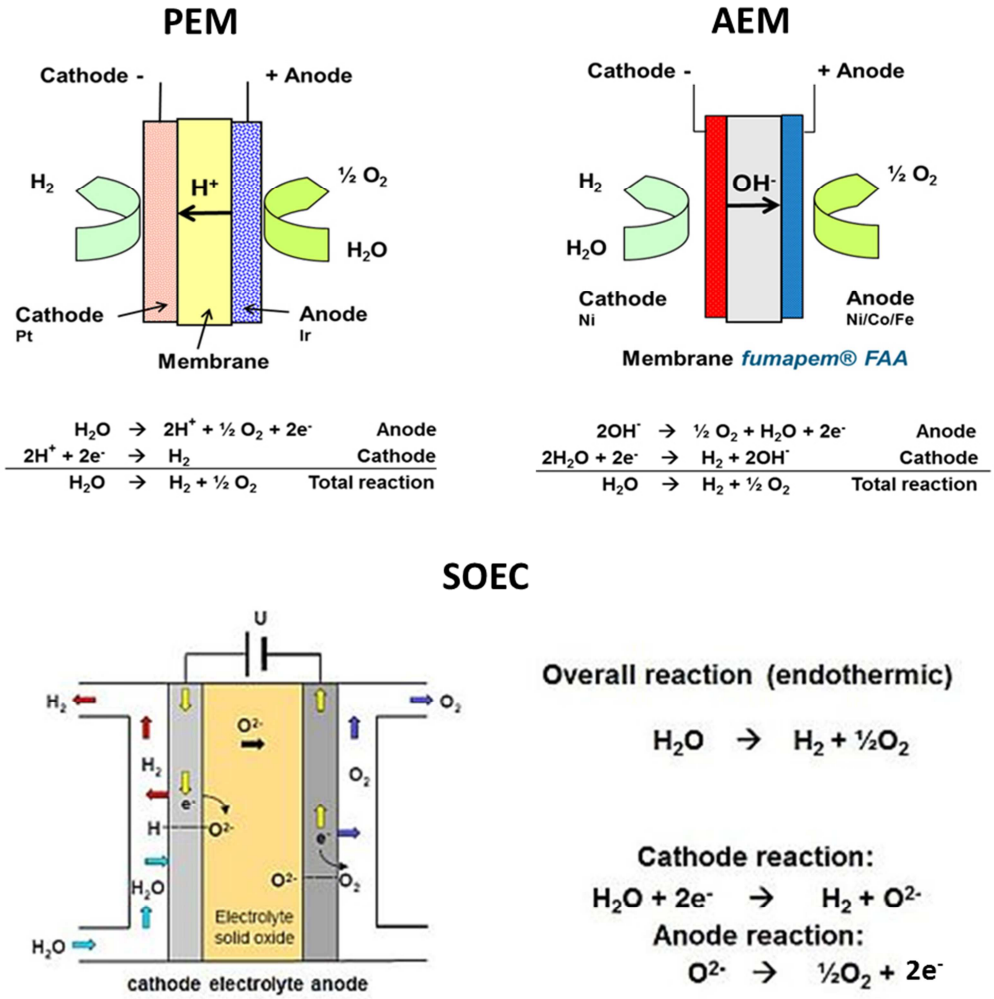

Figure I-6: Schemes of principle of PEM, AEM and SOEC[10,11].

I.3 Photoelectrolysis of water[12]

Photoelectrolysis of water consists in the production of hydrogen and oxygen from water by using solar energy. A similar process able to store solar energy into chemical bonds is already used in the nature: photosynthesis. With the energy from sunlight, plants convert CO_2 and water into hydrocarbons and O_2, however, the yield is very low (<1%)[13]. For the production of hydrogen, we need an artificial process with more efficiency.

Photoelectrolysis of water is carried out in a photoelectrochemical cell (PEC). The PEC is composed of two electrodes and an electrolyte. At the anode, the water is oxidized into oxygen (Equations I.1 and I.3) and, at the cathode, water is reduced into hydrogen (Equations I.2 and I.4). The electrolyte is water but the pH of the water can be modified by adding a base or an acid. The reactions and the redox standard potentials in the two environments are different.

For alkaline electrolyte:

Oxidation (**Equation I.1**):

$4OH^- + 4h^+ \leftrightarrows O_2 + 2H_2O$ $\quad E°_{ox} = -0.401$ V vs. NHE

Reduction (**Equation I.2**):

$4H_2O + 4e^- \leftrightarrows 2H_2 + 4OH^-$ $\quad E°_{red} = -0.828$ V vs. NHE

For acidic electrolyte:

Oxidation (**Equation I.3**):

$2H_2O + 4h^+ \leftrightarrows O_2 + 4H^+$ $\quad E°_{ox} = -1.229$ V vs. NHE

Reduction (**Equation I.4**):

$4H^+ + 4e^- \leftrightarrows 2H_2$ $\quad E°_{red} = 0$ V vs. NHE

The Gibbs energy (ΔG) is an indication of the feasibility of a reaction and is calculated by the equation: $\Delta G=-nF\Delta E$ where n is the number of electrons, F the Faraday constant and ΔE the electrochemical voltage of the reaction.

In the case of the electrolysis of water at standard temperature (298K) and concentrations (1mol/L, 1atm) the electrochemical voltage is ΔE=-1.229V. This corresponds to a Gibbs free energy change of +237kJ/ mol_{H_2}. The reaction of water splitting is thus thermodynamically arduous and necessitates an energy input. In the photoelectrolysis, solar energy will be considered.

The electrochemical voltage of 1.229V is theoretical because it does not take into account the kinetic issues, for example. However, this voltage will be used as reference for the comparison of the performances of different PEC.

I.3.1 Photoelectrochemical cell

In the case of the photoelectrolysis of water, a semiconductor converts photons into electron-hole pairs. These photons must have higher energy than the band gap. Electrons and holes are separated from each other thanks to an electric field.

Holes will be used at the surface of the anode for the oxidation of water into oxygen (Equation I.1 or I.3). Electrons are used at the surface of the cathode for the reduction of water into hydrogen (Equation I.2 or I.4).

In the case of the use of a photoactivated anode (photoanode), the cathode is a metal, generally platinum in order to reduce overvoltage (Figure I-7a). Electrons and holes are photogenerated and separated in the semiconductor of the photoanode. Holes are used at the surface of the photoanode for the oxidation of water and electrons are carried to the conducting support of the semiconductor (generally a transparent conducting oxide film deposited on glass (TCO)) to be transported to the cathode for the reduction of water into hydrogen.

Some groups have also developed photocathodes instead of/or complementary to the photoanode. As it is showed in Figure I-7, different PEC configurations can be envisaged[14]. In this PhD thesis, we have prepared a photoanode and used a platinum wire as counter electrode (cathode) as represented in Figure I-7a. Therefore, this configuration will be explained more in detail.

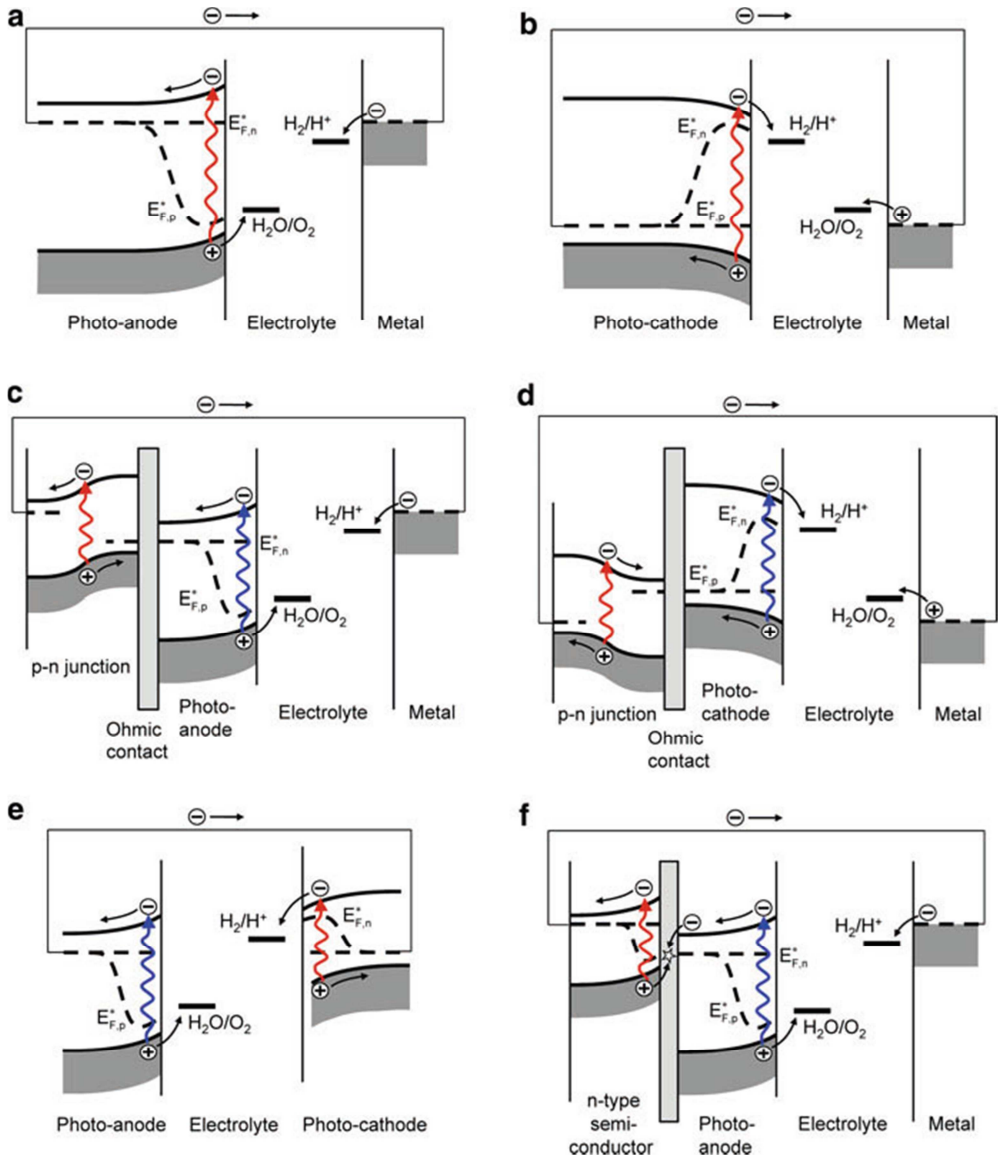

Figure I-7: Possible PEC configurations: ***First row:*** **photoanode (a) or photocathode (b) simply coupled with a metal counter electrode.** ***Second row:*** **photoanode (c) or photocathode (d) biased with an integrated p-n junction.** ***Third row:*** **photoanode coupled with a photocathode (e) or photoanode biased with a second n-type semiconductor (f).** [12]

I.3.2 Working principle[12,14,15]

As mentioned before, electrons and holes generated in the photoanode are separated from each other thanks to an electric field. This electric field appears between the space charge region and the bulk of the semiconductor. It results from the equilibrium between the Fermi level of the photoanode and the redox potential of the electrolyte when the photoanode is put in contact with the electrolyte.

At open circuit, the Fermi level of the photoanode is generally higher than the redox potential of the electrolyte as it can be seen on the left side of Figure I-8. Therefore, electrons are transferred from the photoanode to the electrolyte in order to reduce the position of the Fermi level down to the redox potential value of the electrolyte and reach the equilibrium between them as it is showed in Figure I-8.

Consequently, an upward bending appears in the conduction band and in the valence band of the photoanode. This region in the photoanode is called the space charge region (SCR) as represented on the right side of Figure I-8.

The position of the band edges against the redox potential of the electrolyte is called the flat band potential (V_{fb}). It represents the potential that needs to be applied to the semiconductor to reduce the band bending to zero.

Due to the transfer of charges from the semiconductor to the electrolyte, the surface of the photoanode will be positively charged and the electrolyte in contact will be negatively charged. Once the equilibrium is established, an electric field exists between the space-charge region, also called depletion region, and the bulk of the semiconductor.

The electrolyte will also be affected by this equilibrium. Because of the charge of the photoanode surface, ions with the counter charge will accumulate next to the surface of the semiconductor. The region where there is a gradient of charge in the electrolyte is called the Helmholtz layer (HL) as represented on the right side of Figure I-8.

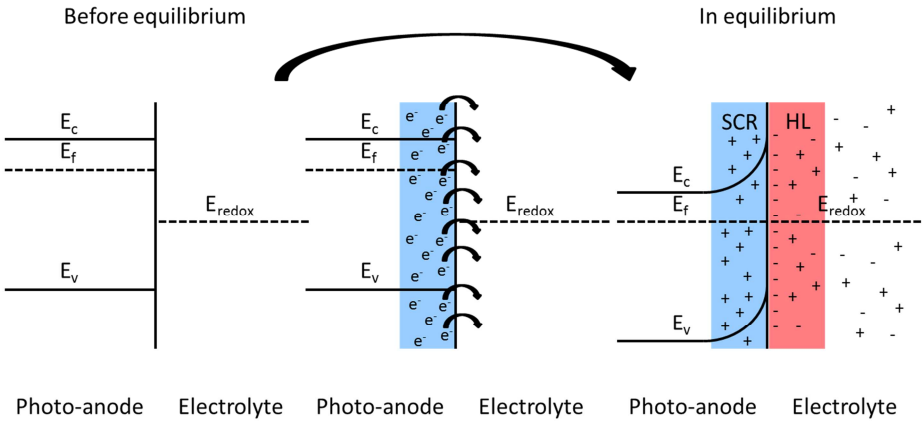

Figure I-8: Evolution of the band diagram of a n-type photoanode in contact with an electrolyte where E_c, E_f, E_v and E_{redox} are respectively the conduction band, Fermi level, valence band and redox potential. SCR is the space-charge region and HL is the Helmholtz layer.

Under illumination, the system is no longer in equilibrium. The creation of electron-hole pairs increases the Fermi level due to the internal photovoltage (ΔV_{photo} represented in Figure I-9). A unique Fermi level cannot chart of the phenomenon near the semiconductor/electrolyte junction and two quasi-Fermi levels are more useful: $E^*_{F,n}$ and $E^*_{F,p}$ (Figure I-9). They are linked to the concentration of electrons and holes according to the position in the photoanode. They only take into account the electrons in the conduction band and holes in the valence band. This limits the predictions in the case of holes trapped at the surface (discrete states).

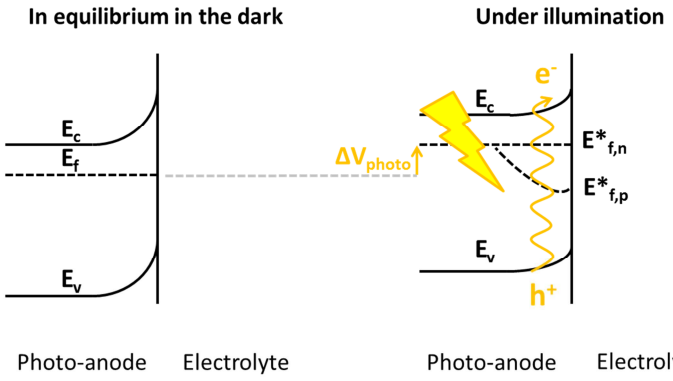

Figure I-9: Band diagram of a PEC in equilibrium in the dark (left) and under illumination (right).

I.3.3 Requirements for photoelectrodes[13,16,17]

Regardless the electrode type, photoelectrodes must satisfy some requirements such as an efficient absorption of the visible light and a good charge transport. The most famous semiconductor meeting these criteria is silicon. However, the efficient absorption of the visible light is not the only requirement; the position of the band gap must overlap the redox potentials of water. As it can be seen on Figure I-10, silicon has a small band gap (1.1 eV) which allows an efficient absorption of the visible light but it does not overlap the redox potentials of water.

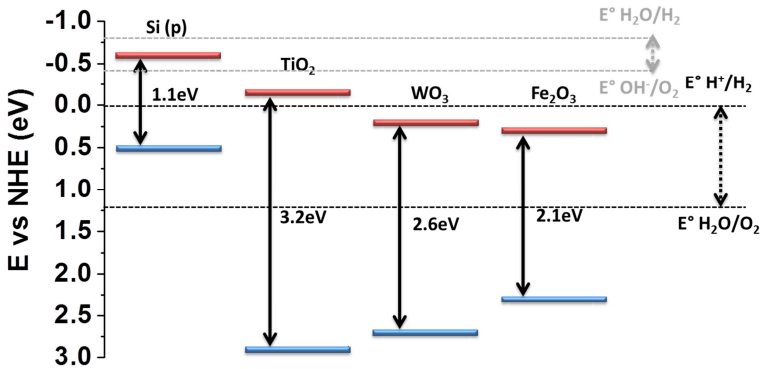

Figure I-10: Standard redox potentials of water in acidic (black dotted lines) and basic (grey dotted lines) media. Band gaps, valence band (blue) and conduction band (red) of Si, TiO_2, WO_3 and Fe_2O_3. Diagram adjusted from publications [18,19]

In 1972, Fujishima and Honda[20] reported the photoelectrolysis of water using a TiO_2 photoanode and a platinum cathode. With TiO_2, the band gap overlaps the redox standard potential of water in acidic media (Figure I-10) but the band gap is higher than 3eV. This means that TiO_2 is absorbing UV radiations which represent a small part of the sunlight.

Since then, there has been a lot of research to find suitable electrode materials in order to use a broader range of the solar spectrum. It is the case for III-V semiconductors materials such as GaAs or other semiconductor such as CdS but they are expensive and not stable in water under anodic conditions[12,17]. Despite the efforts deployed for years, no single material meeting all the requirements of an ideal photoelectrode has emerged[13].

It can be seen on Figure I-10 that WO_3 and Fe_2O_3 can be considered as photoanode but their band gaps do not overlap the reduction potential of water. Despite this issue, WO_3 and Fe_2O_3 are attractive candidates because they are inexpensive and stable in water. If we compare these two oxides in terms of highest potential efficiency, due to its larger band gap, WO_3 has a maximum solar-to-hydrogen (STH) efficiency of 4.8% while a maximum STH of 12.9% could be obtained with Fe_2O_3 (hematite)[21]. Hematite is thus considered as more promising.

I.4 Hematite[17]

Hematite is composed of oxygen and iron, which is an abundant element in the Earth's crust (6.3% by weight). We can find this element in its oxidized forms FeO, Fe_2O_3, Fe_3O_4. Among these oxides, Fe_2O_3 is largely known under the name "rust". Hematite (α-Fe_2O_3) is the most thermodynamically stable crystalline structure and the most used in water splitting. Its crystalline structure is trigonal (hexagonal scalenohedral, $R\bar{3}c$) and is represented in Figure I-11. The anions O^{2-} are organized in a hexagonal closed-packed structure along the [001] (z-axis) direction (Figure I-11a) and the cations Fe^{3+} occupy two third of the octahedral interstices (Figure I-11b).

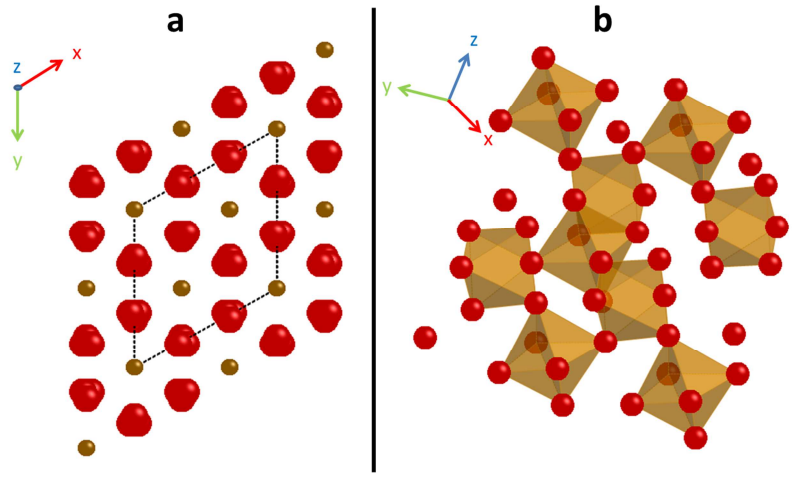

Figure I-11: Crystalline structure of hematite in different orientations to show (a) the hexagonal structure of oxygens and (b) the iron cations situated in the center of two third of octahedra. Oxygen is represented in red and iron in brown. Figure achieved with CrystalMaker®.

The crystalline structure of hematite gives it specific optoelectronic characteristics such as its absorption (Figure I-12). Its transmission in the spectral range from orange to infrared gives its red color.

A slight absorption in the near infrared is attributed to d-d transition states between electron energy levels of the d^5 Fe^{3+} ion. However, the main absorption occurs from ~560-650nm to UV (Figure I-12), where the energy of incident light is equal or higher than the bandgap.

The band gap of hematite is reported between 1.9 eV and 2.2 eV depending on the sample preparation technique. This means that it can theoretically absorb up to 40% of solar radiation[22].

Generally, analyzes from Tauc plots[2] show that the band gap transition is phonon-assisted and thus indirect. Indirect transitions occur less likely than direct transitions because it needs a change in the crystal momentum. This is linked to the smaller absorption of indirect semiconductor. As a consequence, the thickness of indirect semiconductor has to be higher than direct semiconductor to absorb a maximum of the incident light.

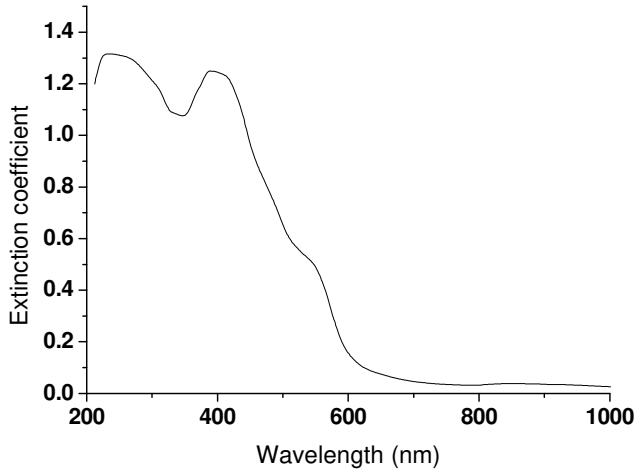

Figure I-12: Extinction coefficient of Hematite to show its absorption as a function of the wavelength.[23]

[2] A Tauc plot is used to determine the optical band gap of a semiconductor

Indirect semiconductors require a high carrier conductivity to transfer charges across the film thickness. Unfortunately, this is not the case for hematite.

When hematite is illuminated, absorbed photons excite electrons from the valence band to the conduction band. Consequently, vacancies are created in the valence band and are designated as holes. Holes can move thanks to the transfer of an electron to the corresponding vacancy.

If the mobility is translated in terms of diffusion length before recombination, holes in hematite have a diffusion length between 1.5nm and 5nm[24,25]. This is very short compared to TiO_2, for example, in which the diffusion length is of the order of 0.1µm for sintered electrodes and of the order of 1µm for single crystal [26]. The very small diffusion length of holes in hematite is an issue for the transfer of holes from the photogeneration area to the semiconductor/electrolyte junction where they are used for the oxidation of water into oxygen.

Electron conductivity in hematite is also very low. The conductivity of holes and electrons in hematite is a "small polarons hopping" conductivity[27-30]. It corresponds to the movement from site to site of the lattice polarization due to the presence of an electron or a hole[31]. Potential wells are created by the displacement of the surrounding atoms due to the movement of a charge carrier. The charge carriers are self-trapped by the potential wells that they create. When surrounding atoms modify their position, a movement of charge carriers is possible. The small polaron conductivity is thus improved when temperature increases[30].

Adding dopants improves the electronic conductivity of the film by increasing the quantity of majority carriers. Depending on the nature of the dopant, a n-type or a p-type hematite can be obtained[17,32,33]. In a p-type semiconductor, holes are the majority carriers and in a n-type semiconductor, electrons are the majority carriers. In hematite, the substitution of Fe^{3+} by a dopant can generate Fe^{2+} sites (n-type semiconductor) or Fe^{4+} sites (p-type semiconductor) to compensate the change of charge[28].

First of all, oxygen vacancies in hematite act as n-type dopant because it generates Fe^{2+} sites. Hematite is known to be a n-type semiconductor because of the natural presence of oxygen vacancies. Moreover, a thermal treatment in an oxygen deficient environment is a doping method that does not necessitate the addition of a heteroatom[34].

The addition of a heteroatom as dopant is another possibility. When Zn^{2+}, Mg^{2+}, Cu^{2+} or Ni^{2+} is added, hematite is converted into a p-type semiconductor because the valence of the cation is smaller than Fe[17,35,36]. But, the examples of p-type doped hematite are less present in the literature.

More publications show an increase of conductivity and performances thanks to a n-type doping of hematite[28,37-41]. A lot of dopants can be used such as Zr^{4+}, Ti^{4+}, Si^{4+}, Sn^{4+}or Ge^{4+} [41-44]. *Ab initio* electron transfer simulations were carried out to compare the effect of a dopant on the electronic conduction in hematite[28]. They predict the increase of charge carrier density due to the presence of the dopant according to its concentration. Concerning the electron transport mode, it can change according to different parameters such as the dopant concentration, the ion size and the ion stability.

The nanostructuration of the photoanode is a strategy to address the short diffusion length of holes[16,17,45]. Instead of improving the conductivity of holes, it is possible to reduce the distance between the generation position of a hole and the semiconductor/liquid junction (SCLJ) at which the oxidation reaction can occur. The nanostructuration has another advantage: the increase of surface sites number for the oxidation of water by increasing the specific surface of the material.

A lot of different nanostructures have been envisaged such as porous thin films[46-48], cauliflowers[38,45], nanotubes[49,50] and nanorods[50,51]. These nanostructures can be obtained by different deposition techniques such as potentiostatic anodization[49], electrodeposition[42,52], chemical vapor deposition at atmospheric pressure (APCVD)[37,53], ultrasonic spray deposition (USP)[54,55] and spin coating[48,56,57].

The mechanism of water oxidation is not well understood. However, the four-hole water oxidation process is known to be very slow[58]. Therefore, to improve holes collection for water oxidation instead of recombination with electrons, hematite films request the deposition of a catalyst on the surface. The catalyst will improve the kinetic of water oxidation and thus favor this reaction instead of the recombination between holes and electrons. A lot of reports on cobalt-, nickel- or iridium- based catalysts such as IrO_2[45], cobalt-phosphate (Co-Pi)[59,60], CoO_x[61], $NiFeO_x$[61] and NiO_x[62] have been published. The objective is to find a catalyst with a high efficiency, a high durability and based on abundant elements for the purpose of a large scale development of PEC.

The wide variety of parameters, such as dopant, catalyst, thickness and conditions of measurement (pH, light source…), affecting the performances of a photoanode makes the comparison difficult. Currently, the highest performance reported in the literature is around 3 mA/cm^2 (at 1.23 V vs reference hydrogen electrode) for a nanostructured hematite film containing a dopant to improve conductivity and a catalyst to reduce the overpotential[45].

In conclusion, hematite is a promising material for the photoanode in water splitting but it suffers from different recombination mechanisms[13] located in the bulk and at the surface, limiting the efficiencies of charge generation (η_{e^-/h^+}), transport (η_{tr}) and charge transfer (η_{ct}) as it is shown in Figure I-13. These phenomena reduce the performances of the PEC. In order to increase the η_{e^-/h^+} and η_{tr}, hematite films must be thick enough but the path distance of charges must be reduced and the conduction improved. It can be achieved thanks to the addition of a dopant and by working on nanostructuration of the film. To reduce the recombination at the surface and then increase η_{ct}, the kinetic of water oxidation must be improved with a catalyst.

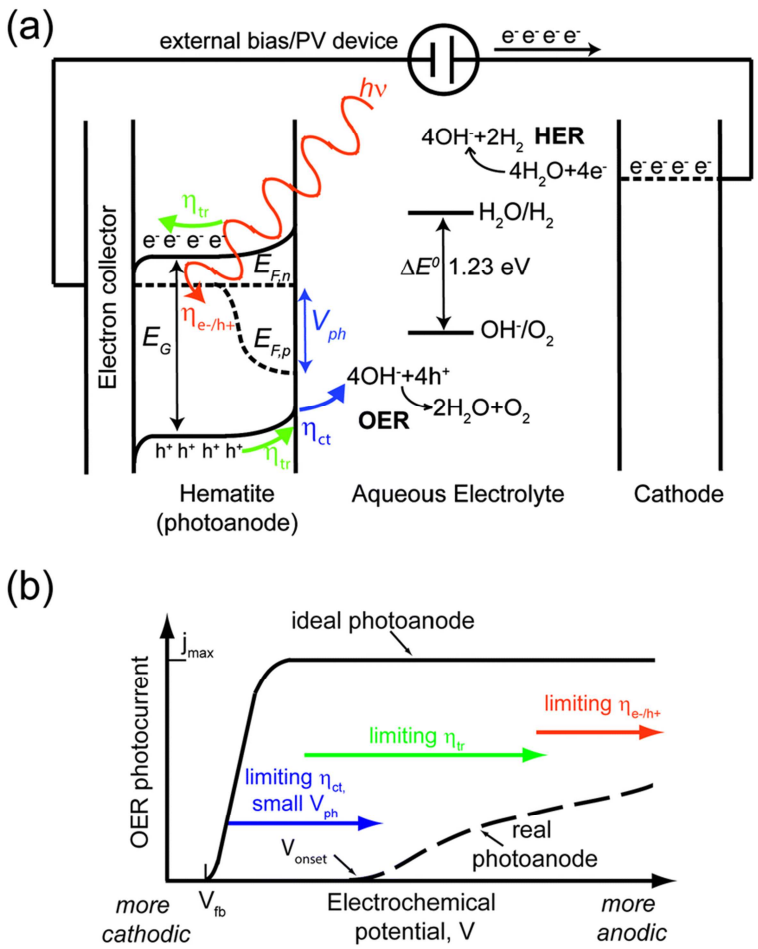

Figure I-13: (a) schematic energy diagram of a PEC based on a hematite photoanode and a metallic cathode. HER means "Hydrogen Evolution Reaction" and OER "Oxygen Evolution Reaction". Photons (hv) with energy equal to or higher than the band gap (E_g) are absorbed by the photoanode and converted in electron/hole pairs with efficiency (η_{e^-/h^+}). Thanks to the electric field generated in the space charge region, electron and holes are separated. Holes move to the photoanode/electrolyte junction and electrons move toward the cathode (via an electron collector and an external circuit). η_{tr} (transport efficiency) is the fraction of photogenerated charges reaching the respective solid-liquid interface. Moreover, holes are transferred to the electrolyte with a charge transfer efficiency η_{ct} to oxidize water into oxygen. An external bias or a PV device is used for the transfer of electrons to the cathode for the reduction of water into hydrogen. (b) The difference in terms of photocurrent between the actual best efficiency according to the state of the art is represented by the dotted line and the ideal performance of a PEC based on a hematite photoanode is represented by the solid line. The arrows indicate the limiting factors to the reduction of the onset potential.[13]

I.5 Objectives of the thesis

As explained in the first part of this chapter, greenhouse gas emissions must be reduced and hydrogen is an alternative to the use of fossil fuel. A low carbon footprint technique to produce it is the photoelectrolysis of water.

Hematite is a promising material for the photoanode but suffers from different drawbacks: poor electronic conductivity, short diffusion length of holes and kinetics issues for water oxidation into oxygen. The goal of this thesis is to design a hematite photoanode with optimized nanostructure and improved charge carriers' conductivity.

Indeed, it is not mandatory to improve the diffusion length of holes. As mentioned before, another considered strategy is the reduction of holes path distance from the generation site to the semiconductor/electrolyte junction where they are used for the water oxidation.

Mesoporosity induces a higher specific surface and allows a deeper penetration of the electrolyte into the film compared to a dense film. This reduces the pathway of holes. In order to demonstrate the impact of the mesostructure on the performances of the film, a comparison between dense and mesoporous film was carried out.

We have optimized the nanostructure of the photoanode by a templating approach to prepare mesoporous hematite films. Soft-templating is a common technique already implemented in our group for the preparation of porous metal oxide such as TiO_2[63,64], LiV_2O_5[65], $Nb_{2x}V_{2-2x}O_5$[66]. The challenge was to adapt this technique to the preparation of hematite because the crystallization temperature of hematite is relatively high (450°C)[67] compared to other oxides such as TiO_2 anatase (350°C)[63].

For the improvement of electron conductivity, the solution envisaged in the literature is the doping. As explain in the previous section, a lot of different dopants can be used. We have decided to add titanium because the sol-gel chemistry of titanium oxide is compatible with the soft-templating process. As for the mesoporosity, films with and without dopant were tested in order to highlight the modifications induced by the addition of a dopant.

The performances, in terms of photocurrent obtained with the different films, were evaluated in order to identify the best procedure for the preparation of an efficient Ti-doped mesoporous hematite film. Moreover, other measurements such as TEM, XRD or EIS were performed in order to justify this best procedure compared to the others.

I.6 Structure of the manuscript

The different topics listed in the objectives are developed more in detail in six chapters. The content of these chapters is summarized here after.

The general context and the objectives of the research were presented in Chapter I.

Chapter II describes the different steps of the elaboration of a doped mesoporous hematite film. Specifically, the templating and the transformation of a hybrid film into a crystallized doped hematite film are reported.

Chapter III is dedicated to the study of the microstructure effect on the performances of the film. Three different microstructures are compared: dense, collapsed and mesoporous.

Chapter IV analyzes the impact of the presence of a dopant in the hematite films. Performances of doped and undoped films are compared. Moreover, impedance spectroscopy measurements were performed on different films to give some clarifications about the differences observed in terms of photocurrent.

Chapter V presents perspectives of further developments of mesoporous hematite films. Specifically, measurements were carried out in a "holes scavenger medium" (H_2O_2) to simulate the efficiencies that could be obtained with a catalyst deposited onto the surface of optimized mesoporous Ti-doped hematite films. Besides, we report a mesoporous film prepared by ultrasonic spray pyrolysis, which is a deposition technique more transposable to the industry.

Finally, the last chapter takes up the key points of the different chapters of the manuscript and gives some recommendations for future research works.

I.7 References

(1) GIEC: *Changements climatiques 2014: rapport de synthèse. Contribution des Groupes de travail I,II et III au cinquième Rapport d'évaluation du Groupe d'experts intergouvernemental sur l'évolution du climat*; GIEC: Genève, Suisse, **2014**.

(2) IEA: *Technology Roadmap: Hydrogen and Fuel Cells*; OECD/IEA, **2015**.

(3) IEA: *Tracking Clean Energy Progress 2015*; OECD/IEA, 2015.

(4) Hyundai: *ix 35 Fuel Cell* Available from http://worldwide.hyundai.com/WW/Showroom/Eco/ix35-Fuel-Cell/PIP/index.html. **2016**

(5) Meyer, P. E.; Winebrake, J. J.: Modeling technology diffusion of complementary goods: The case of hydrogen vehicles and refueling infrastructure. *Technovation* **2009**, *29*, 77-91.

(6) Mortreux, A.; Petit, F.: *Industrial Applications of Homogeneous Catalysis*; Springer Netherlands, 1988.

(7) Bhandari, R.; Trudewind, C. A.; Zapp, P.: Life cycle assessment of hydrogen production via electrolysis - A review. *Journal of Cleaner Production* **2014**, *85*, 151-163.

(8) Ball, M.; Wietschel, M.: The future of hydrogen – opportunities and challenges. *International Journal of Hydrogen Energy* **2009**, *34*, 615-627.

(9) Ebbesen, S. D.; Jensen, S. H.; Hauch, A.; Mogensen, M. B.: High Temperature Electrolysis in Alkaline Cells, Solid Proton Conducting Cells, and Solid Oxide Cells. *Chemical Reviews* **2014**, *114*, 10697-10734.

(10) Vogt, U.; Braun, A.: Hydrogen Production, (Solar) Water splitting ; Available from http://oldweb.empa.ch/plugin/template/empa/3/*/---/l=1. http://oldweb.empa.ch/plugin/template/empa/3/*/---/l=1, **2015**.

(11) Energiespeicher: New membrane materials for PEM water electrolysis; Available from http://forschung-energiespeicher.info/en/projektschau/gesamtliste/projekt-einzelansicht/95/Neue_Membranmaterialien_fuer_die_PEM_Wasserelektrolyse/. http://forschung-energiespeicher.info/en/projektschau/gesamtliste/projekt-einzelansicht/95/Neue_Membranmaterialien_fuer_die_PEM_Wasserelektrolyse/, **2016**.

(12) Van de Krol, R.; Grätzel, M.: *Photoelectrochemical Hydrogen Production*; Springer US, 2012.

(13) Iandolo, B.; Wickman, B.; Zoric, I.; Hellman, A.: The rise of hematite: origin and strategies to reduce the high onset potential for the oxygen evolution reaction. *Journal of Materials Chemistry A* **2015**, *3*, 16896-16912.

(14) Walter, M. G.; Warren, E. L.; McKone, J. R.; Boettcher, S. W.; Mi, Q.; Santori, E. A.; Lewis, N. S.: Solar Water Splitting Cells. *Chemical Reviews* **2010**, *110*, 6446-6473.

(15) Nozik, A. J.; Memming, R.: Physical Chemistry of Semiconductor−Liquid Interfaces. *The Journal of Physical Chemistry* **1996**, *100*, 13061-13078.

(16) Lin, Y.; Yuan, G.; Liu, R.; Zhou, S.; Sheehan, S. W.; Wang, D.: Semiconductor nanostructure-based photoelectrochemical water splitting: A brief review. *Chem. Phys. Lett.* **2011**, *507*, 209-215.

(17) Sivula, K.; Le Formal, F.; Graetzel, M.: Solar Water Splitting: Progress Using Hematite (α -Fe_2O_3) Photoelectrodes. *ChemSusChem* **2011**, *4*, 432-449.

(18) Gratzel, M.: Photoelectrochemical cells. *Nature* **2001**, *414*, 338-344.

(19) Krawicz, A.; Cedeno, D.; Moore, G. F.: Energetics and efficiency analysis of a cobaloxime-modified semiconductor under simulated air mass 1.5 illumination. *Physical Chemistry Chemical Physics* **2014**, *16*, 15818-15824.

(20) Fujishima, A.; Honda, K.: Electrochemical photolysis of water at a semiconductor electrode. *Nature* **1972**, *238*, 37-8.

(21) Murphy, A. B.; Barnes, P. R. F.; Randeniya, L. K.; Plumb, I. C.; Grey, I. E.; Horne, M. D.; Glasscock, J. A.: Efficiency of solar water splitting using semiconductor electrodes. *International Journal of Hydrogen Energy* **2006**, *31*, 1999-2017.

(22) Marusak, L. A.; Messier, R.; White, W. B.: Optical absorption spectrum of hematite, α-Fe_2O_3 near IR to UV. *Journal of Physics and Chemistry of Solids* **1980**, *41*, 981-984.

(23) Sokolik, I. N.; Toon, O. B.: Incorporation of mineralogical composition into models of the radiative properties of mineral aerosol from UV to IR wavelengths. *Journal of Geophysical Research: Atmospheres* **1999**, *104*, 9423-9444.

(24) Sastri, M. V. C.; Nagasubramanian, G.: Studies on ferric oxide electrodes for the photo-assisted electrolysis of water. *International Journal of Hydrogen Energy* **1982**, *7*, 873-876.

(25) Le Formal, F.; Tetreault, N.; Cornuz, M.; Moehl, T.; Graetzel, M.; Sivula, K.: Passivating surface states on water splitting hematite photoanodes with alumina overlayers. *Chem. Sci.* **2011**, *2*, 737-743.

(26) Salvador, P.: Hole diffusion length in n-TiO_2 single crystals and sintered electrodes: Photoelectrochemical determination and comparative analysis. *Journal of Applied Physics* **1984**, *55*, 2977-2985.

(27) Liao, P.; Carter, E. A.: Hole transport in pure and doped hematite. *Journal of Applied Physics* **2012**, *112*, 013701.

(28) Liao, P.; Toroker, M. C.; Carter, E. A.: Electron transport in pure and doped hematite. *Nano Lett.* **2011**, *11*, 1775-1781.

(29) Boumaza, S.; Boudjemaa, A.; Omeiri, S.; Bouarab, R.; Bouguelia, A.; Trari, M.: Physical and photoelectrochemical characterizations of hematite α-Fe_2O_3: Application to photocatalytic oxygen evolution. *Solar Energy* **2010**, *84*, 715-721.

(30) Rettie, A. J. E.; Chemelewski, W. D.; Emin, D.; Mullins, C. B.: Unravelling Small-Polaron Transport in Metal Oxide Photoelectrodes. *The Journal of Physical Chemistry Letters* **2016**, *7*, 471-479.

(31) Cox, P. A.: *Transition metal oxides : An introduction to their electronic structure and properties*; Oxford University Press, 1992.

(32) Calleja, G.; Serrano, D. P.; Sanz, R.; Pizarro, P.: Mesostructured SiO_2-doped TiO_2 with enhanced thermal stability prepared by a soft-templating sol–gel route. *Microporous and Mesoporous Materials* **2008**, *111*, 429-440.

(33) Saremi-Yarahmadi, S.; Wijayantha, K. G. U.; Tahir, A. A.; Vaidhyanathan, B.: Nanostructured α-Fe_2O_3 Electrodes for Solar Driven Water Splitting: Effect of Doping Agents on Preparation and Performance. *J. Phys. Chem. C* **2009**, *113*, 4768-4778.

(34) Ling, Y.; Wang, G.; Reddy, J.; Wang, C.; Zhang, J. Z.; Li, Y.: The Influence of Oxygen Content on the Thermal Activation of Hematite Nanowires. *Angewandte Chemie International Edition* **2012**, *51*, 4074-4079.

(35) Malviya, K. D.; Dotan, H.; Shlenkevich, D.; Tsyganok, A.; Mor, H.; Rothschild, A.: Systematic comparison of different dopants in thin film hematite (α-Fe_2O_3) photoanodes for solar water splitting. *Journal of Materials Chemistry A* **2016**, *4*, 3091-3099.

(36) Mirbagheri, N.; Wang, D.; Peng, C.; Wang, J.; Huang, Q.; Fan, C.; Ferapontova, E. E.: Visible Light Driven Photoelectrochemical Water Oxidation by Zn- and Ti-Doped Hematite Nanostructures. *ACS Catalysis* **2014**, *4*, 2006-2015.

(37) Cesar, I.; Kay, A.; Gonzalez, M. J. A.; Graetzel, M.: Translucent Thin Film Fe_2O_3 Photoanodes for Efficient Water Splitting by Sunlight: Nanostructure-Directing Effect of Si-Doping. *J. Am. Chem. Soc.* **2006**, *128*, 4582-4583.

(38) Cesar, I.; Sivula, K.; Kay, A.; Zboril, R.; Gratzel, M.: Influence of Feature Size, Film Thickness and Silicon Doping on the Performance of Nanostructured Hematite Photoanodes for Solar Water Splitting. *J. Phys. Chem. C* **2009**, *113*, 772-782.

(39) Cho, S.; Jang, J.-W.; Lee, K.-H.; Lee, J. S.: Research Update: Strategies for efficient photoelectrochemical water splitting using metal oxide photoanodes. *APL Materials* **2014**, *2*, 010703.

(40) Chou, J.-C.; Lin, S.-A.; Lee, C.-Y.; Gan, J.-Y.: Effect of bulk doping and surface-trapped states on water splitting with hematite photoanodes. *Journal of Materials Chemistry A* **2013**, *1*, 5908-5914.

(41) Glasscock, J. A.; Barnes, P. R. F.; Plumb, I. C.; Savvides, N.: Enhancement of Photoelectrochemical Hydrogen Production from Hematite Thin Films by the Introduction of Ti and Si. *J. Phys. Chem. C* **2007**, *111*, 16477-16488.

(42) Kumar, P.; Sharma, P.; Shrivastav, R.; Dass, S.; Satsangi, V. R.: Electrodeposited zirconium-doped α-Fe_2O_3 thin film for photoelectrochemical water splitting. *Int. J. Hydrogen Energy* **2011**, *36*, 2777-2784.

(43) Liu, J.; Liang, C.; Zhang, H.; Tian, Z.; Zhang, S.: General Strategy for Doping Impurities (Ge, Si, Mn, Sn, Ti) in Hematite Nanocrystals. *The Journal of Physical Chemistry C* **2012**, *116*, 4986-4992.

(44) Ling, Y.; Wang, G.; Wheeler, D. A.; Zhang, J. Z.; Li, Y.: Sn-Doped Hematite Nanostructures for Photoelectrochemical Water Splitting. *Nano Lett.* **2011**, *11*, 2119-2125.

(45) Tilley, S. D.; Cornuz, M.; Sivula, K.; Graetzel, M.: Light-Induced Water Splitting with Hematite: Improved Nanostructure and Iridium Oxide Catalysis. *Angew. Chem., Int. Ed.* **2010**, *49*, 6405-6408, S6405/1-S6405/3.

(46) Ahn, H. J.; Kwak, M. J.; Lee, J. S.; Yoon, K. Y.; Jang, J. H.: Nanoporous hematite structures to overcome short diffusion lengths in water splitting. *Journal of Materials Chemistry A* **2014**, *2*, 19999-20003.

(47) Brillet, J.; Gratzel, M.; Sivula, K.: Decoupling Feature Size and Functionality in Solution-Processed, Porous Hematite Electrodes for Solar Water Splitting. *Nano Lett.* **2010**, *10*, 4155-4160.

(48) Guo, L.; Ida, S.; Takashiba, A.; Daio, T.; Teramae, N.; Ishihara, T.: Soft-templating method to synthesize crystalline mesoporous α-Fe_2O_3 films. *New Journal of Chemistry* **2014**, *38*, 1392-1395.

(49) Mohapatra, S. K.; John, S. E.; Banerjee, S.; Misra, M.: Water Photooxidation by Smooth and Ultrathin α-Fe_2O_3 Nanotube Arrays. *Chem. Mater.* **2009**, *21*, 3048-3055.

(50) Mao, A.; Shin, K.; Kim, J. K.; Wang, D. H.; Han, G. Y.; Park, J. H.: Controlled synthesis of vertically aligned hematite on conducting substrate for photoelectrochemical cells: nanorods versus nanotubes. *ACS Appl. Mater. Interfaces* **2011**, *3*, 1852-1858.

(51) Beermann, N.; Vayssieres, L.; Lindquist, S. E.; Hagfeldt, A.: Photoelectrochemical Studies of Oriented Nanorod Thin Films of Hematite. *J. Electrochem. Soc.* **2000**, *147*, 2456-2461.

(52) Kleiman-Shwarsctein, A.; Hu, Y.-S.; Forman, A. J.; Stucky, G. D.; McFarland, E. W.: Electrodeposition of α-Fe_2O_3 Doped with Mo or Cr as Photoanodes for Photocatalytic Water Splitting. *J. Phys. Chem. C* **2008**, *112*, 15900-15907.

(53) Zhang, P.; Kleiman-Shwarsctein, A.; Hu, Y.-S.; Lefton, J.; Sharma, S.; Forman, A. J.; McFarland, E.: Oriented Ti doped hematite thin film as active photoanodes synthesized by facile APCVD. *Energy Environ. Sci.* **2011**, *4*, 1020-1028.

(54) Duret, A.; Grätzel, M.: Visible Light-Induced Water Oxidation on Mesoscopic α-Fe_2O_3 Films Made by Ultrasonic Spray Pyrolysis. *J. Phys. Chem. B* **2005**, *109*, 17184-17191.

(55) Henrist, C.; Toussaint, C.; de Vroede, J.; Chatzikyriakou, D.; Dewalque, J.; Colson, P.; Maho, A.; Cloots, R.: Surfactant-assisted ultrasonic spray pyrolysis of hematite mesoporous thin films. *Microporous and Mesoporous Materials* **2016**, *221*, 182-186.

(56) Frydrych, J.; Machala, L.; Tucek, J.; Siskova, K.; Filip, J.; Pechousek, J.; Safarova, K.; Vondracek, M.; Seo, J. H.; Schneeweiss, O.; Gratzel, M.; Sivula, K.; Zboril, R.: Facile fabrication of tin-doped hematite photoelectrodes - effect of doping on magnetic properties and performance for light-induced water splitting. *J. Mater. Chem.* **2012**, *22*, 23232-23239.

(57) Souza, F. L.; Lopes, K. P.; Nascente, P. A. P.; Leite, E. R.: Nanostructured hematite thin films produced by spin-coating deposition solution: Application in water splitting. *Sol. Energy Mater. Sol. Cells* **2009**, *93*, 362-368.

(58) Sivula, K.: Metal Oxide Photoelectrodes for Solar Fuel Production, Surface Traps, and Catalysis. *J. Phys. Chem. Lett.* **2013**, *4*, 1624-1633.

(59) Barroso, M.; Cowan, A. J.; Pendlebury, S. R.; Grätzel, M.; Klug, D. R.; Durrant, J. R.: The Role of Cobalt Phosphate in Enhancing the Photocatalytic Activity of α-Fe_2O_3 toward Water Oxidation. *J. Am. Chem. Soc.* **2011**, *133*, 14868-14871.

(60) Zhong, D. K.; Cornuz, M.; Sivula, K.; Gratzel, M.; Gamelin, D. R.: Photo-assisted electrodeposition of cobalt-phosphate (Co-Pi) catalyst on hematite photoanodes for solar water oxidation. *Energy Environ. Sci.* **2011**, *4*, 1759-1764.

(61) Trotochaud, L.; Ranney, J. K.; Williams, K. N.; Boettcher, S. W.: Solution-Cast Metal Oxide Thin Film Electrocatalysts for Oxygen Evolution. *Journal of the American Chemical Society* **2012**, *134*, 17253-17261.

(62) Young, K. M. H.; Hamann, T. W.: Enhanced photocatalytic water oxidation efficiency with $Ni(OH)_2$ catalysts deposited on α-Fe_2O_3 via ALD. *Chemical Communications* **2014**, *50*, 8727-8730.

(63) Dewalque, J.; Cloots, R.; Mathis, F.; Dubreuil, O.; Krins, N.; Henrist, C.: TiO_2 multilayer thick films (up to 4 mm) with ordered mesoporosity: Influence of template on the film mesostructure and use as high efficiency photoelectrode in DSSCs. *Journal of Materials Chemistry* **2011**, *21*, 7356-7363.

(64) Dewalque, J.; Cloots, R.; Dubreuil, O.; Krins, N.; Vertruyen, B.; Henrist, C.: Microstructural evolution of a TiO_2 mesoporous single layer film under calcination: Effect of stabilization and repeated thermal treatments on the film crystallization and surface area. *Thin Solid Films* **2012**, *520*, 5272-5276.

(65) Caes, S.; Malherbe, C.; Krins, N.; Arrebola, J. C.; Henrist, C.; Cloots, R.; Vertruyen, B.: Lithium transition metal (Ti, Nb, V) oxide mesoporous thin films: Contrasting results when attempting direct synthesis by evaporation-induced self assembly. *Microporous and Mesoporous Materials* **2013**, *172*, 87-94.

(66) Krins, N.; Lepot, L.; Cloots, R.; Vertruyen, B.: Structural and electrochemical characterization of mesoporous thin films of $Nb_{2x}V_{2-2x}O_5$ upon lithium intercalation. *Solid State Ionics* **2009**, *180*, 848-852.

(67) Brezesinski, T.; Groenewolt, M.; Antonietti, M.; Smarsly, B.: Crystal-to-Crystal Phase Transition in Self-Assembled Mesoporous Iron Oxide Films. *Mesoporous Materials* **2006**, *45*, 781-784.